Nanoscale

RSC Publishing

COMMUNICATION

View Article Online
View Journal | View Issue

Cite this: *Nanoscale*, 2013, **5**, 1483

Received 23rd October 2012
Accepted 18th December 2012

DOI: 10.1039/c2nr33294a

www.rsc.org/nanoscale

Synthesis of a CdSe–graphene hybrid composed of CdSe quantum dot arrays directly grown on CVD-graphene and its ultrafast carrier dynamics†

Yong-Tae Kim,[a] Hee-Won Shin,[b] Young-Seon Ko,[c] Tae Kyu Ahn*[b] and Young-Uk Kwon*[ac]

We report the original fabrication and performance of a photocurrent device that uses directly grown CdSe quantum dots (QDs) on a graphene basal plane. The direct junction between the QDs and graphene and the high quality of the graphene grown by chemical vapor deposition enables highly efficient electron transfer from the QDs to the graphene. Therefore, the hybrids show large photocurrent effects with a fast response time and shortened photoluminescence (PL) lifetime. The PL lifetime quenching can be explained as being due to the efficient electron transfer as evidenced by femtosecond transient absorption spectroscopy. These hybrids are expected to find applications in flexible electronics and optoelectronic devices.

Introduction

The ability of graphene to exchange electrons or energy with other materials or molecules is attracting broad interest.[1–3] In particular, many authors have reported on the photophysical properties of hybrids of graphene and CdSe quantum dots (QDs).[4–10] The photoluminescence (PL) of CdSe QDs in these hybrids is reduced both in intensity and lifetime, which is indicative of energy transfer from the QDs to the graphene.[6] Photovoltaic[7] and large photocurrent effects also have been reported for such hybrids,[11,12] which is indicative of electron transfer.

However, strictly speaking, all of the CdSe QD–graphene hybrids investigated so far have one or more problems in their representations of the intrinsic nature of the interaction between QDs and graphene. First and most of all, the hybrids are based on graphene oxide (GO) or reduced graphene oxide (rGO), not intrinsic graphene. Although GO and rGO share some common features with graphene, their band structures and electronic properties are completely different from those of graphene. GO and rGO are semiconductors and resistive while graphene is semimetallic and conductive. With large numbers of functional groups and high densities of defects, GO and rGO are chemically reactive while the graphene basal plane is inert. Second, most of the QDs used in the syntheses of hybrids are surface-modified by organic capping agents, which exert the effects of an insulator and/or a spacer affecting the interaction between the QD and the graphene. It is clear that unless the QDs are free of capping agent and intrinsic graphene is used the properties of the QD–graphene hybrid are bound to be influenced by one or more extraneous factors.

There have been two exceptions to these general observations. Brus *et al.* and Klekachev *et al.* have studied the interaction between intrinsic graphene and core–shell type CdSe@ZnS QDs.[13,14] They used intrinsic graphene, single layer graphene obtained by peeling off graphite, and the QDs were placed on the graphene surface by dispersing colloidal QD solutions. From the study on the PL properties of the QDs in contact with the graphene, Brus *et al.* concluded that the energy of the photoexcited QDs was transferred to graphene through the Föster resonance energy transfer (FRET) mechanism.[13] They also argued that the electron transfer in their system was negligible because of the energy barrier of the ZnS shell and the lack of chemical bonding between the QDs and the graphene. On the other hand, Klekachev *et al.*, through measurements on a field effect transistor (FET) fabricated with QD-deposited graphene, showed that there was electron transfer in addition to the FRET mechanism.[14]

[a]*SKKU Advanced Institute of Nanotechnology (SAINT), Center for Human Interface Nano Technology (HINT), Sungkyunkwan University, Suwon 440-746, Korea. E-mail: tanatos@skku.edu; Fax: +82 31 299 4179; Tel: +82 31 290 5970*

[b]*Department of Energy Science, Sungkyunkwan University, Suwon, 440-476, Korea. E-mail: taeahn@skku.edu; Fax: +82 31 299 4279; Tel: +82 31 299 6270*

[c]*Department of Chemistry, BK-21 School of Chemical Materials Sciences, Sungkyunkwan University, Suwon 440-746, Korea. E-mail: ywkwon@skku.edu; Fax: +82 31 299 4179; Tel: +82 31 290 7070*

† Electronic supplementary information (ESI) available: TEM data of MSTF, AFM data of T-QD–G samples, PL decay fitting results to the multiexponential decay equation, photoconductivity data of T-QD–2LG with two different illumination wavelengths, photocurrent efficiencies of QD–G hybrids prepared in various ways, photoconductivity and photoresponse data of T-QD–2LG and T-QD–3LG, and the bending stress on a PET film. See DOI: 10.1039/c2nr33294a

Apparently, the interaction between QDs and graphene occurs through both energy and electron transfer mechanisms. The relative weights of the two mechanisms will be strongly dependent on the material's design.

In this paper, we synthesized CdSe QD–graphene hybrid materials whose design was optimised for the electron transfer mechanism between QDs and intrinsic graphene. The hybrid was prepared on a graphene sheet grown on a Cu substrate by chemical vapor deposition (CVD)[15] and the CdSe QDs were deposited electrochemically with a mesoporous silica thin film (MSTF) template (pore diameter ~8 nm).[16] This hybrid had some unique features that are unprecedented in the study of related materials: (1) the use of CVD graphene, as opposed to rGO,[4–12] provides the opportunity to study the effect of the intrinsic properties of graphene free from the effects of defects and the inter-sheet junctions of rGO. The same effect may be achieved with graphene produced by the peeling off method, but CVD graphene is far more advantageous for forming large area devices. (2) The QDs form a monolayer on the graphene surface with the QDs regularly ordered with gaps between adjacent QDs, which rules out the possibility of the effect of inter-QD interactions. (3) The QDs are directly in contact with the graphene surface. The details of the fabrication and characterization are discussed below.

Experimental section

The fabrication of CdSe QDs–graphene samples in this study consisted of the synthesis of graphene (step (a) in Fig. 1), the transfer of graphene to a substrate (b), the formation of an MSTF on graphene (c and e), the electrochemical deposition of CdSe QDs, and the removal of the MSTF template (d and f). Depending on the purpose, Au electrodes can be formed on the MSTF before the deposition of CdSe QDs (e).

The graphene film was synthesized by the CVD method on Cu foil.[15,17] A piece of Cu foil of 25 μm in thickness was placed in a quartz tube under an argon atmosphere. The temperature was raised to 1000 °C in an H_2 flow (10 sccm), and then in a flow of a reaction gas mixture of CH_4 (15 sccm) and H_2 (10 sccm). After the growth, the temperature was lowered at the rate of *ca.* 10 °C s^{-1}. The graphene on the back-side was removed by O_2 plasma after protecting the front-side with a polymethylmethacrylate (PMMA) coating. The graphene film was transferred onto a quartz or polyethylene terephtalate (PET) substrate after the Cu foil was etched in an ammonium persulfate solution. Finally, the graphene–quartz film was heated at 180 °C for 1 h in air to enhance the adhesion of graphene to the substrate.

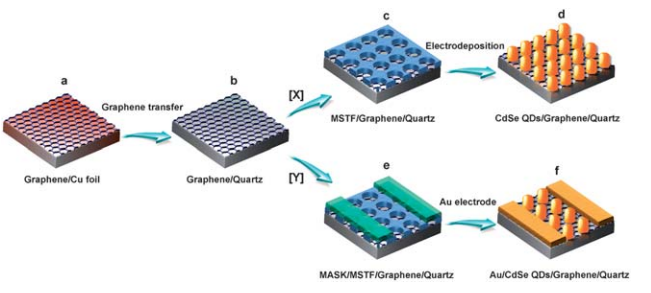

Fig. 1 Schematic drawing of the procedure to fabricate CdSe QD–G hybrids (path X) and a photocurrent measurement device of CdSe QD–G (path Y): (a) growth of a monolayer graphene sheet by chemical vapor deposition, (b) transfer of the graphene sheet onto a quartz substrate using a PMMA layer as a sample handle, (c) synthesis of an MSTF on the graphene on quartz, (d) electrodeposition of CdSe into the pores of the MSTF followed by the removal of MSTF, (e) PTEF mask formation on the MSTF–graphene followed by deposition of CdSe on selected areas, and (f) deposition of Au electrodes onto the graphene away from the CdSe deposited area.

The precursor solution of an MSTF[18] was prepared by dissolving tetraethoxyorthosilicate (TEOS, 99.999%) and a Pluronic triblock copolymer (F-127) in a mixed solution of diluted aqueous HCl and absolute ethanol resulting in the composition TEOS : F-127 : HCl : H_2O : EtOH = 1 : 6.60 × 10^{-3} : 6.66 × 10^{-3} : 4.62 : 22.6 (molar ratio). The solution was stirred at 20 °C for 18 h under a controlled relative humidity of below 20% before use. The solution was spin-coated onto the graphene–quartz substrate, aged at 80 °C, and calcined at 400 °C to form the MSTF template.

A corner of the MSTF film on the graphene–quartz was etched out to reveal the graphene surface to make an electrical contact with a wire for the following electrochemical deposition. Using MSTF-coated graphene as the working electrode, Ag/AgCl (KCl sat'd) as the reference electrode and Pt as the counter electrode in a three-electrode cell and an aqueous electrolyte solution (0.3 M $CdSO_4$, 0.003 M SeO_2), CdSe was deposited under a constant potential of −0.7 V at 50 °C. After the deposition, the MSTF template was removed by dissolving in an aqueous 0.2 wt% HF solution.

Field-emission scanning electron microscopy (SEM; JEOL JSM-7100F, 5–10 kV), high-resolution transmission electron microscopy (TEM; JEOL JEM-3010, 300 kV) and atomic force microscopy (AFM, Park systems XE-100; non-contact mode) were used to characterize the samples for the morphology. UV-vis absorption spectra were obtained on a Shimadzu UV-3600. Raman spectra were recorded with a Renishaw RM-1000 Invia using an excitation wavelength of 514 nm and a notch filter of 50 cm^{-1}. The spectral resolution was 0.2 cm^{-1}. PL lifetimes were measured on a conventional time-correlated single photon counting (TCSPC) system (PicoQuant GmbH, FluoTime 200). The light source was a picosecond diode laser of 485 nm with 4 MHz repetition (PicoQuant GmbH, LDH-P-C-485, power: 0.6 mW). The instrumental response function (IRF) was *ca.* 160 ps (FWHM). The cutoff filters were applied to the emission light to remove any trace of scattering and the emission light was aligned with a magic angle (54.7°) to the excitation laser pulse. In order to monitor electron transfer, pump-probe femtosecond transient absorption (TA) experiments were carried out using a commercial Helios system (Ultrafast Systems). The pump beam of 490 nm with a pulse energy of 1.6 μJ was obtained from an optical parametric amplifier (Light conversion, TOPAS-C), pumped by a regeneratively amplified Ti:sapphire laser system (Coherent, Libra). The probe pulse was a white light continuum generated by focusing a small portion of the amplifier output though a sapphire window. Photoconductivity measurements were performed under the illumination of a 300 W Xe lamp.

Results and discussion

The synthesis procedure is illustrated in Fig. 1. Graphene was synthesized by CVD on Cu foil, which is known to produce mostly monolayers (>98%) of graphene.[15,17] After the growth, the graphene (1.5 × 1.5 cm^2) was transferred onto a quartz substrate (2 × 2 cm^2) or a PET film using a PMMA over-coating following the reported method.[19] This process was repeated to form bi- or tri-layer graphene films (hereafter, 2LG and 3LG, respectively). The resistivity of 2LG and 3LG were measured as 400 and 330 Ω $\square^{-1}$, respectively, by the four probe method, which agree with the literature values.[20] An MSTF was formed on graphene as a template.[16] This template consisted of regularly ordered vertical pores with hexagonal symmetry when viewed from the top (Fig. S1†). The pore size was ~8 nm and the wall thickness was 4 nm.[18,21] CdSe QDs were formed inside the pores by electrochemical deposition. After the deposition, the MSTF template was removed with diluted HF to reveal the array structure of the CdSe QDs on the graphene (path X in Fig. 1: a → b → c → d). We used 2LG or 3LG on a quartz substrate to form this structure. Monolayer graphene had the problems of low conductivity and poor mechanical properties, and thus was not used.

For comparative purposes, we also prepared a hybrid by dispersing CdSe QDs on the graphene surface. A commercial CdSe QDs solution (Aldrich, Lumidot 640; ~6.6 nm in size) was dispersed on the surface of 2LG or 3LG by spin-casting followed by drying. The amount of QDs was controlled to be the same as in the hybrid formed using the above-mentioned templating method. Hereafter, the sample produced by the template synthesis will be called T-QD–G and the one by dispersion D-QD–G.

The device for the photoconductivity measurements was fabricated following the procedure outlined in Fig. 1 (path Y: a → b → e → f). A polytetrafluoroethylene (PTFE) seal tape was applied on the MSTF template to define the area where CdSe QDs were to be deposited. After the MSTF template was removed, Au electrodes were deposited on the QD-free areas (Fig. 2(A)). The graphene in this device was 1.5 × 1.5 cm^2 in area and the QD-deposited region in the center was 1 × 1 cm^2. The same device with D-QD–G was also fabricated for comparison.

The SEM image of the CdSe QD-deposited area in Fig. 2(C) shows an array structure of the CdSe QDs on the graphene. Uniform-sized QDs in a hexagonal array with ~4 nm gaps between adjacent QDs can be seen. The top-view TEM image of the graphene plane in Fig. 2(D) shows that the QDs are single crystals. The electron diffraction pattern of this sample could be indexed with the wurtzite-type lattice.[16] The lattice fringes marked in Fig. 2(D) are identified as the (110) planes of the hexagonal unit cell. Because the (110) planes are perpendicular to the graphene plane, the QDs grow with their (001) planes parallel to the basal plane of the graphene. It has been reported that CdS and CdSe nanoparticles can grow epitaxially on carbon nanotubes or graphene (GO and rGO) surfaces by sharing the (001) planes. The interaction between the nanoparticles and the graphene is chemical in nature involving the orbitals of the Cd(II) ions and the π orbitals of the graphene carbon atoms.[22]

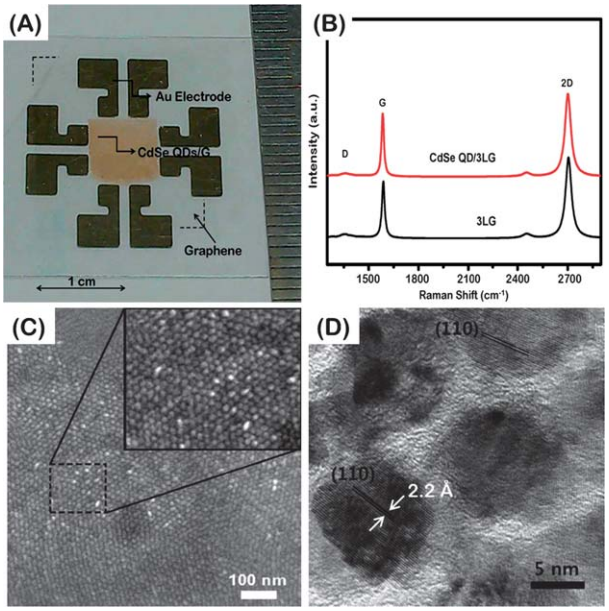

Fig. 2 (A) A photograph of the device fabricated by path Y in Fig. 1. (B) Raman spectra of graphene before and after the deposition of CdSe QDs on the quartz substrate. (C) SEM image of CdSe QDs grown on graphene. The inset is a magnified view. (D) TEM image of CdSe QDs grown on graphene. The lattice fringes are the (110) planes of wurtzite CdSe.

Therefore, it is highly possible that the QDs in our hybrid samples also grow epitaxially on the graphene surface. The AFM data show that the QDs are about 20 nm in height (Fig. S2†).

The Raman spectra of 3LG before and after the deposition of CdSe QDs are compared in Fig. 2(B). The positions of the G- and 2D-bands at 1585 and 2703 cm^{-1}, respectively, and the intensity ratio between the G and 2D bands (I(G)/I(2D) = 0.7) of 3LG agree with the literature data on stacked graphene.[23] This and the low intensity of the D-band peak indicate that our graphene was of high quality.[15,17] The deposition of the QDs does not induce any significant level of defect formation in the graphene, indicated by the fact that I(G)/I(2D) and the intensity of the D-band peak are not changed in the spectrum of T-QD–3LG. However, the G and 2D bands of T-QD–3LG are red-shifted by ~2 cm^{-1} from those of 3LG, indicating electron doping. The red-shifts were confirmed by repeating the measurements on at least 15 different samples (Fig. S3†).

Fig. 3(A) shows the UV-vis spectra of D-QD–G and T-QD–G. The suspension solution of the CdSe QDs used to form D-QD–G shows a peak at 625 nm which agrees with the particle size of 6.6 nm reported by the supplier. The peak position is not changed upon forming D-QD–G indicating that the QD–graphene interaction does not induce any significant change in the electronic state of the QDs. T-QD–G shows an absorption peak at 660 nm, which can be explained by the larger size of the QDs than in D-QD–G. The peak intensities of T-QD–G and D-QD–G are similar to each other because the amounts of QDs in both samples have been controlled to be the same.

To monitor the photophysical properties, we measured the PL lifetimes of the QD–G samples as shown in Fig. 3(B). In the case of the QDs dispersed on quartz, the QDs show an average

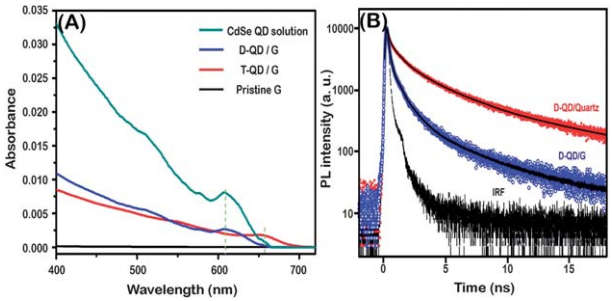

Fig. 3 (A) Absorption spectra of T-QD–G and D-QD–G. (B) PL decay profiles of D-QD on quartz and graphene substrates. Decay curve of T-QD–G is not shown because it is indistinguishable from the IRF.

PL lifetime of 6.6 ns. On forming a thin layer on graphene (D-QD–G), the average PL lifetime is decreased to 2.1 ns (Table S1†). Similar results have been reported for CdSe@ZnS dispersed on graphene (from 20 ns to 0.25 ns)[13] and for surface passivated CdSe QDs attached to GO (from 4.4 ns to 1.6 ns),[7] which are explained as being due to FRET. In sharp contrast, T-QD–G does not show any meaningful PL trace. Because the T-QD–G samples show detectable absorption in the UV-vis spectrum, the absence of a PL trace indicates ultrafast energy quenching by graphene beyond the detection limit of our instrument of a few tens of ps.

In order to closely study the decay dynamics, we utilized femtosecond TA spectroscopy. TA spectra of T-QD–G at different time delays are shown in Fig. 4(A). Since it is not possible for the near-infrared (NIR) probe energy (λ = 850–1300 nm) to induce absorption across the band gap of the CdSe QDs, the observed signals must have originated from the photoexcited electrons and holes.[24] Recently, Weiss *et al.* have shown that the NIR-TA of CdSe QDs (5.0 nm in size) in solution is composed of three major components, each with distinctly different lifetimes.[25] The first and second fastest processes with lifetimes of 2–5 ps and 30–50 ps respectively are attributed to the decay of relaxed excitonic states of the CdSe QDs. Fig. 4(B) shows the normalized decay profiles of D-QD–G (blue squares) and T-QD–G (red circles) probed at 1100 nm. Decay time constants were obtained by convoluting the measured signal with the cross-correlated Gaussian function of 200 fs (FWHM). The decay curves were

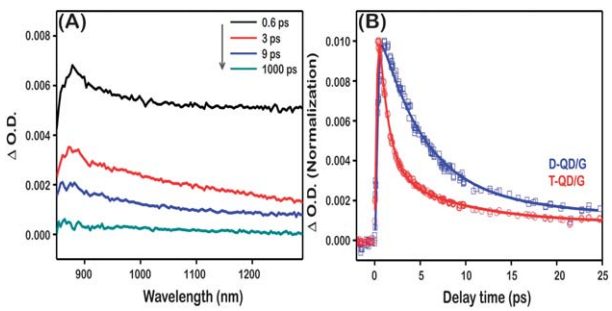

Fig. 4 (A) Transient absorption spectra of T-QD–G at the indicated time delays following a 490 nm excitation pulse. (B) Normalized decay profiles of D-QD–G and T-QD–G probed at 1100 nm. The fitting results are shown as solid lines.

fitted to get biexponential functions within 25 ps time delay. The convoluted time constants for T-QD–G are τ_1 = 1.06 ps (77%) and τ_2 = 8.35 ps (23%) and those for D-QD–G are τ_1 = 4.57 ps (80%) and τ_2 = 13.2 ps (20%). The weighted average lifetime ($\tau_{avg} = \Sigma_i A_i\tau_i/\Sigma_i A_i$) of T-QD–G (2.7 ps) is much shorter than that of D-QD–G (6.3 ps).

Based on the assignment of Weiss *et al.* these components correspond to the decay kinetics of the relaxed excitonic states of the QDs.[25] Since it has been already demonstrated by Klekachev *et al.* that CdSe@ZnS QDs inject photoexcited electrons into intrinsic graphene,[14] the facilitated decays seen in our TA spectra can be attributed to the electron transfer from the CdSe QDs to the graphene. Compared with the data on suspended QDs by Weiss *et al.* our sample showed shorter lifetimes, indicative of efficient electron transfer. Considering that the lifetimes of QDs tend to increase with size and that the QDs in our samples are larger,[26] ~8 × 8 × 20 nm^3 (T-QD–G) and 6.6 nm (D-QD–G), the effect of electron transfer on our hybrids is very significant. Remarkably, T-QD–G shows a decay process more than four times faster than D-QD–G despite the large size difference. We believe the ultrafast electron transfer in T-QD–G is the consequence of the high charge carrier mobility of intrinsic graphene and the strong coupling between the QDs and graphene through the direct contacts. The ultrafast charge carrier dynamics in T-QD–G explains the absence of its PL signal.

More direct proof for the electron transfer would be provided by the transport properties under illumination. FET measurements with illumination as reported by Klekachev *et al.*[14] would be the most desirable. However, unfortunately, the synthesis procedure of T-QD–G which involves wet-chemistry processes is not compatible with the fabrication process for an FET device. We therefore chose to measure the photoconductivity properties of T-QD–G with visible illumination. Intrinsic graphene does not show any photocurrent under visible light illumination because of the very low visible light absorption by graphene (2.3% per layer),[27,28] which we also have verified (Fig. S4†).

The photocurrent properties of intrinsic graphene have been reported, but all studies are under infrared illumination.[22] Moreover, all such cases utilize the internal field generated at the Schottky junction between graphene and the metal electrodes.[29–33] Therefore, any photocurrent effect of a symmetric device of QD–G with visible light can be attributed to the electron transfer from the QDs.

The *I–V* characteristics of the T-QD–G and D-QD–G samples under white illumination by a 300 W Xe lamp and in the dark are shown for 2LG (Fig. 5(A)) and 3LG (Fig. 5(B)). The T-QD–G samples show about double the photocurrent of the D-QD–G ones in both cases. The results are summarized in Fig. 5(C). The devices with 3LG are better than those with 2LG in terms of the photocurrent efficiency by about 50%. This seems to be related to the lower resistivity of 3LG than that of 2LG. In addition, the mobility of the charge carriers in graphene increases with the increase in the number of layers. Although the 2LG and 3LG in the present study do not have the stacking properties of as-grown multilayer graphene, there may be interlayer interactions

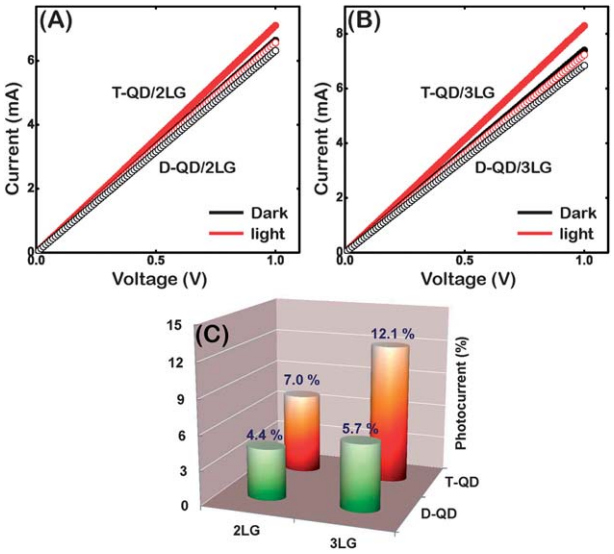

Fig. 5 *I–V* characteristics of T-QD–G and D-QD–G devices fabricated with (A) 2LG and (B) 3LG. (C) Comparison of photocurrent efficiency among the measured QD–G devices.

to increase the mobility as the number of layers increases. By contrast, illumination of intrinsic graphene does not result in any change in the *I–V* plot from that in the dark (Fig. S4†). The enhanced photoconductivity of T-QD–G can be well explained by ultrafast electron transfer as proved by the TA spectroscopy data.

We also studied the photoresponses of T-QD–G with monochromatic light of wavelengths shorter or longer than the absorption edge of the QDs, 660 nm. Under illumination with $\lambda = 405$ nm, T-QD–G showed an increased current in its *I–V* plot. However, when 670 nm photons were used, the *I–V* curve was unchanged from that in the dark (Fig. S5†). Therefore, T-QD–G devices exhibit photocurrent through the absorption of photons by CdSe QDs.

In the literature, there are two examples of QD–rGO hybrids whose photodetection properties have been measured.[11,12] In one case in which the CdSe QDs are surface-passivated by a capping agent, a photocurrent effect of less than 10% was achieved.[11] Compared with this result, our system has ~1000 times higher material efficiency. In the other case in which the QDs are in direct contact with rGO, the device showed a 17-fold increase in current upon illumination.[12] However, since rGO films show photoconductivity which is attributed to the recombination properties of electron–hole pairs in sp^2 cluster-like states between overlapping rGO flakes,[34] the major part of the photoconductivity effect on rGO-based materials cannot be attributed to the intrinsic properties of the QD–graphene interaction.

Finally, we also studied the possibility of fabricating a flexible electrode of our T-QD–G. A CdSe QD–G film was transferred onto a PET substrate to check the variation in photoresponse during the bending process. When the sample was bent by about 44°, the photoresponse efficiency was slightly decreased by ~0.6% (Fig. S6†).

Conclusion

In conclusion, we have synthesized a novel CdSe QD–graphene hybrid which is composed of densely arrayed wurtzite-type CdSe QDs in direct contact with the graphene basal plane. As a result of the effect of the combination of the high quality of the graphene and the direct contact, our T-QD–G hybrids show ultrafast quenching of the PL of the CdSe QDs. The PL quenching can be explained as being due to efficient electron transfer. Our hybrid demonstrates an improved materials design over the existing ones for obtaining enhanced electron transfer from QDs to graphene. Because the sizes of the devices based on T-QD–G are practically unlimited, we believe that they can find applications in photovoltaic devices.

Acknowledgements

We thank CCRF for the TEM and EDX data. We thank Drs S. H. Seol and H. S. Han in SAIT for femtosecond TA setup. We thank Prof. B. H. Hong at Seoul National University for the kind donation of graphene. This work was supported by grants NRF-2011-0031392 (Priority Research Center Program), NRF-2009-0083540 (Basic Science Research Program), NRF-20090081018 (Basic Science Research Program), NRF-2010-0010610 (Basic Science Research Program), 2011-0031565 (Global Frontier R&D Program), and R31-10029 (World Class University Program). TKA also acknowledges TJ Park POSCO science fellowship.

Notes and references

1 K. K. Manga, Y. Zhou, Y. Yan and K. P. Loh, *Adv. Funct. Mater.*, 2009, **19**, 3638.
2 J. M. Yun, J. S. Yeo, J. W. Kim, H. G. Jeong, D. Y. Kim, Y. J. Noh, S. S. Kim, B. C. Ku and S. I. Na, *Adv. Mater.*, 2011, **23**, 4923.
3 Z. Liu, Q. Liu, Y. Huang, Y. Ma, S. Yin, X. Zhang, W. Sun and Y. Chen, *Adv. Mater.*, 2008, **20**, 3924.
4 P. V. Kamat, *J. Phys. Chem. Lett.*, 2011, **2**, 242.
5 I. V. Lightcap and P. V. Kamat, *J. Am. Chem. Soc.*, 2012, **134**, 7109.
6 A. F. Zedan, S. Sappal, S. Moussa and M. S. El-Shall, *J. Phys. Chem. C*, 2010, **114**, 19920.
7 J. Chen, F. Xu, J. Wu, K. Qasim, Y. Zhou, W. Lei, L. T. Sun and Y. Zhang, *Nanoscale*, 2012, **4**, 441.
8 X. Zhang, S. Li, X. Jin and S. Zhang, *Chem. Commun.*, 2011, **47**, 4929.
9 Y. Ye, L. Gan, Y. Dai, X. Guo, H. Meng, B. Yu, Z. Shi, K. Shang and G. Qin, *Nanoscale*, 2011, **3**, 1477.
10 Y. Wang, H. B. Yao, X. H. Wang and S. H. Yu, *J. Mater. Chem.*, 2011, **21**, 562.
11 X. Geng, L. Niu, Z. Xing, R. Song, G. Liu, M. Sun, G. Cheng, H. Zhong, Z. Liu, Z. Zhang, L. Sun, H. Xu, L. Lu and L. Liu, *Adv. Mater.*, 2010, **22**, 638.
12 Y. Lin, K. Zhang, W. Chen, Y. Liu, Z. Geng, J. Zeng, N. Pan, L. Yan, X. Wang and J. G. Hou, *ACS Nano*, 2010, **4**, 3033.
13 Z. Chen, S. Berciaud, C. Nuckolls, T. F. Heinz and L. E. Brus, *ACS Nano*, 2010, **4**, 2964.

14 A. V. Klekachev, M. Cantoro, M. H. Van der veen, A. L. Stesmans, M. M. Heyns and S. De gendt, *Physica E*, 2011, **43**, 1046.
15 X. S. Li, W. W. Cai, J. H. An, S. Kim, J. Nah, D. X. Yang, R. Piner, A. Velamakanni, I. Jung, E. Tutuc, S. K. Banerjee, L. Colombo and R. S. Ruoff, *Science*, 2009, **324**, 1312.
16 Y. T. Kim, J. H. Han, B. H. Hong and Y. U. Kwon, *Adv. Mater.*, 2010, **22**, 515.
17 S. K. Bae, H. K. Kim, Y. B. Lee, X. Xu, J. S. Park, Y. Zheng, J. Balakrishnan, T. Lei, H. R. Kim, Y. I. Song, Y. J. Kim, K. S. Kim, BŐzyilmaz, J. H. Ahn, B. H. Hong and S. Iijima, *Nat. Nanotechnol.*, 2010, **5**, 574.
18 U. H. Lee, J. H. Yang, H. J. Lee, J. Y. Park, K. R. Lee and Y. U. Kwon, *J. Mater. Chem.*, 2008, **18**, 1881.
19 X. S. Li, W. W. Cai, L. Colombo and R. S. Ruoff, *Nano Lett.*, 2009, **9**, 4268.
20 J. M. Kang, S. H. Hwang, J. H. Kim, M. H. Kim, J. C. Gyu, S. J. Seo, B. H. Hong, M. K. Kim and J. B. Choi, *ACS Nano*, 2012, **6**, 5360.
21 K. R. Lee and Y. U. Kwon, *Nano*, 2010, **5**, 75.
22 B. H. Juárez, C. Klinke, A. Kornowski and H. Weller, *Nano Lett.*, 2007, **7**, 3564.
23 A. C. Ferrari and J. Robertson, *Phys. Rev. B: Condens. Matter Mater. Phys.*, 2001, **64**, 075414.
24 E. A. McArthur, A. J. Morris-Cohen, K. E. Knowles and E. A. Weiss, *J. Phys. Chem. B*, 2010, **114**, 14514.
25 K. E. Knowles, E. A. McArthur and E. A. Weiss, *ACS Nano*, 2011, **5**, 2026.
26 A. Kongkanand, K. Tvrdy, K. Takechi, M. Kuno and P. V. Kamat, *J. Am. Chem. Soc.*, 2008, **130**, 4007.
27 A. B. Hungría, B. H. Juárez, C. Klinke, H. Weller and P. A. Midgley, *Nano Res.*, 2008, **1**, 89.
28 H. Liang, W. Ren, J. Su and C. Cai, *Thin Solid Films*, 2012, **521**, 163.
29 T. Mueller, F. Xia and P. Avouris, *Nat. Photonics*, 2010, **4**, 297.
30 F. Xia, T. Mueller, Y. M. Lin, A. Valdes-Garcia and P. Avouris, *Nat. Nanotechnol.*, 2009, **4**, 839.
31 J. Park, Y. H. Ahn and C. Ruiz-Vargas, *Nano Lett.*, 2009, **9**, 1742.
32 F. Xia, T. Mueller, R. Golizadeh-Mojarad, M. Freitag, Y. M. Lin, J. Tsang, V. Perebeinos and P. Avouris, *Nano Lett.*, 2009, **9**, 1039.
33 F. T. Vasko and V. Ryzhii, *Phys. Rev. B: Condens. Matter Mater. Phys.*, 2008, **77**, 195433.
34 C. T. Chien, S. S. Li, W. J. Lai, Y. C. Yeh, H. A. Chen, I. S. Chen, L. C. Chen, K. H. Chen, T. Nemoto, S. Isoda, M. Chen, T. Fujita, G. Eda, H. Yamaguchi, M. Chhowalla and C. Wei Chen, *Angew. Chem., Int. Ed.*, 2012, **51**, 6662.

